

Plate 1 Use of scanned archive aerial photographs, digital photogrammetry and GIS to plot river channel erosion along the Afon Trannon, Wales (part of the study by Mount et al 2000, 2003).

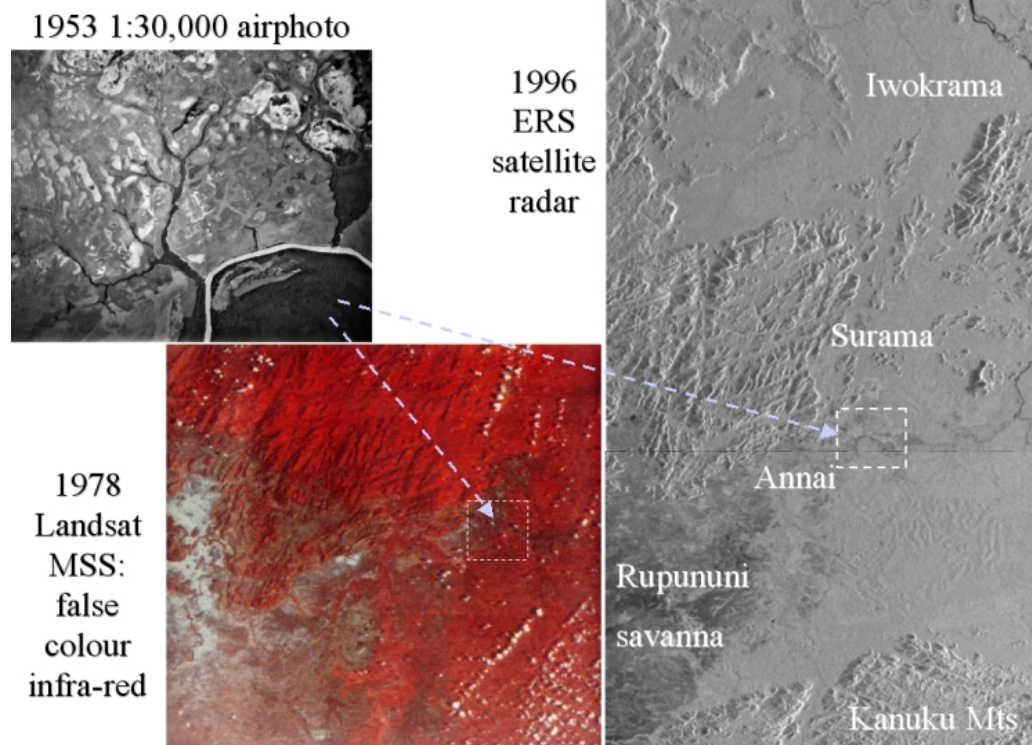


Plate 2 Part of the rainforest-savanna boundary in Guyana, viewed from three different sensors: panchromatic aerial photography, false-colour infra-red Landsat MSS and radar from the ERS-1 satellite (courtesy of the European Space Agency).



Plate 3 Do-it-yourself aerial photography: shot from the window of a passenger aircraft in West Africa, using Kodak Ektachrome infra-red film. Chlorophyll-rich vegetation shows as dark tones, distinguishing lush, often forested, valley swamps from dry grasslands (grey) and bare soil (white).

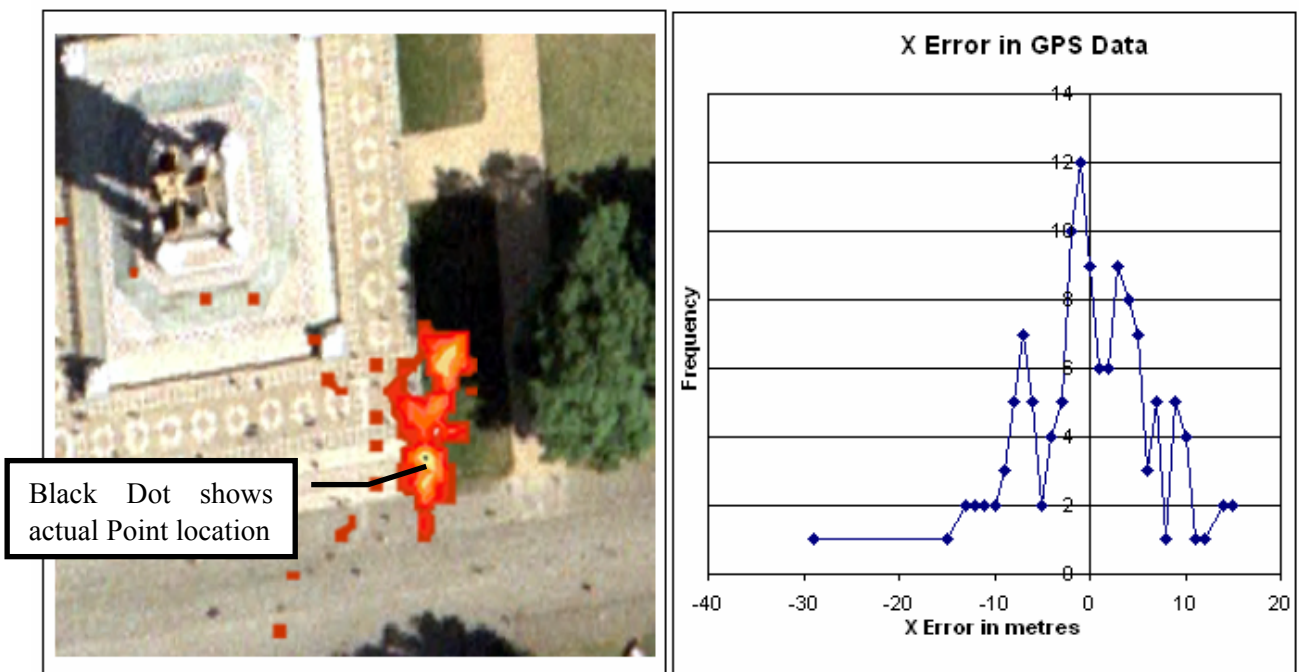


Plate 4 GPS error. Left hand diagram shows a colour coded frequency distribution of GPS results around a location. The lighter the red colour the more times the GPS reported that location. Spread approximately 35 m X and 25 m Y. Apart from two tails of data in the X dimension, X values are grouped very tightly together (within 5 m). Y values fluctuate more (15 m). The diagram to the right shows this more clearly with a cross section through the X axis. The cross section shows an almost Gaussian distribution. Dropouts are most likely due to insufficient data points.

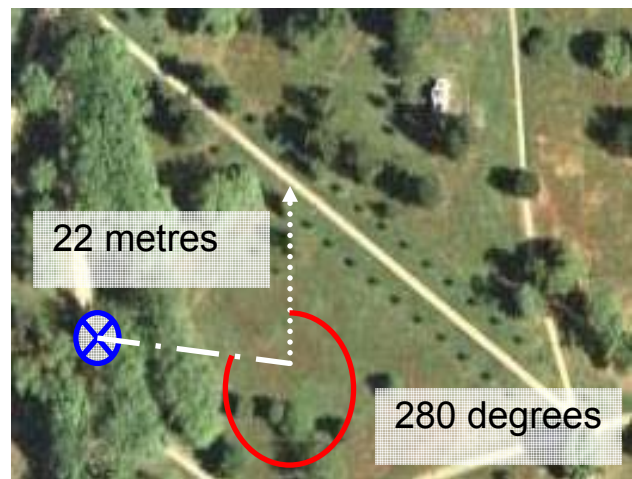
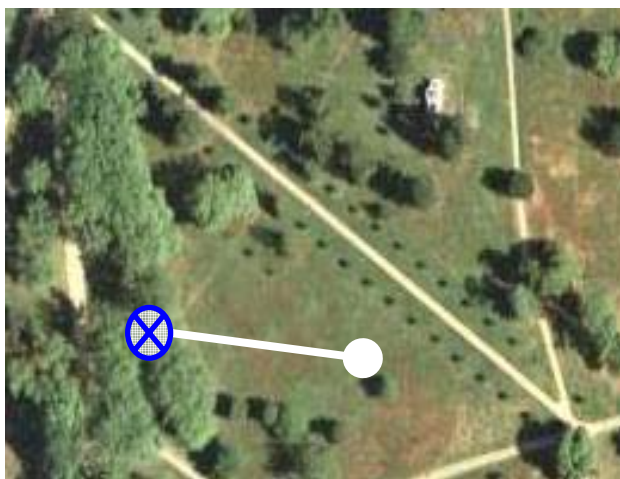
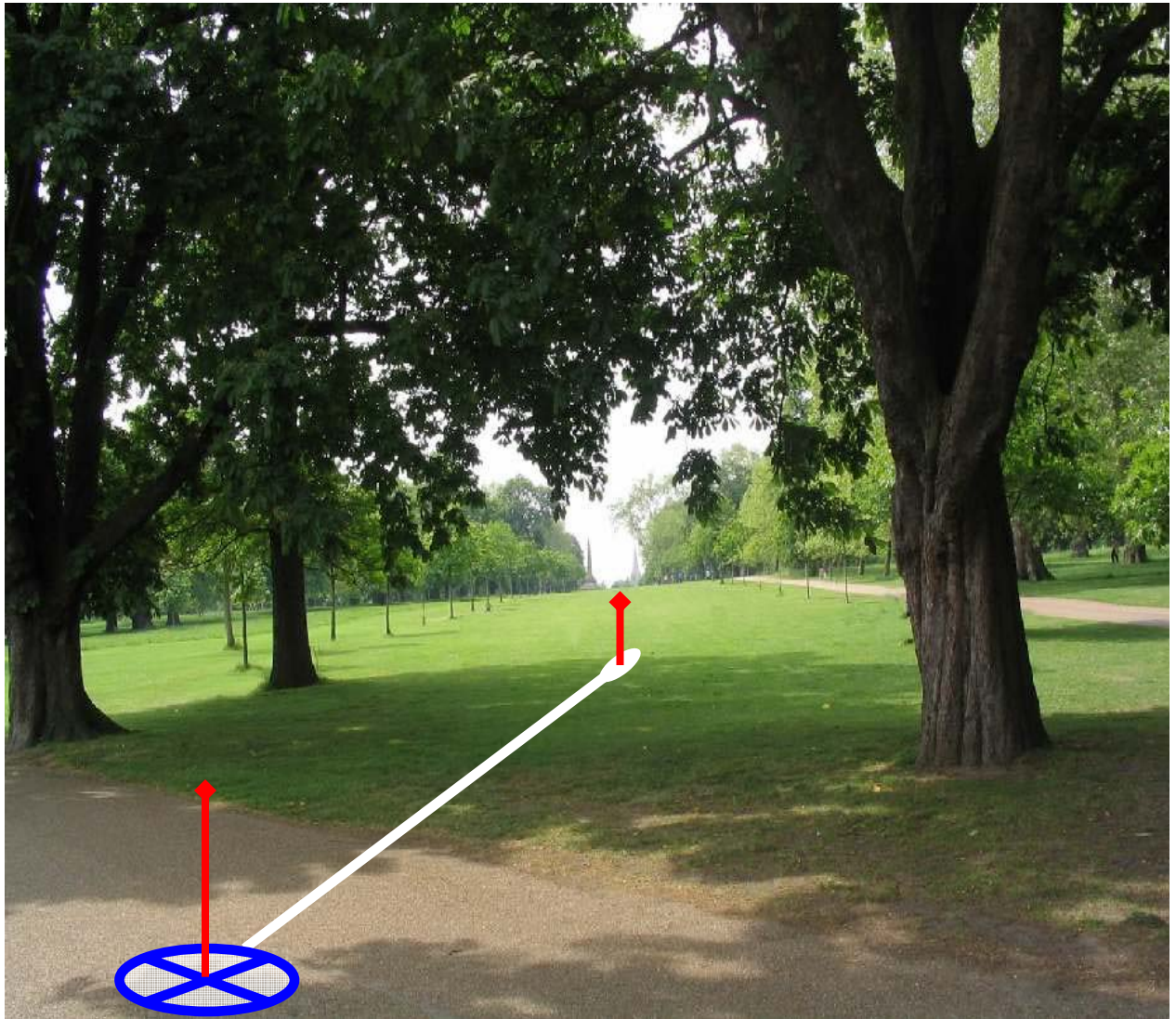


Plate 5 Using surveying techniques with a GPS to improve fixes in difficult locations. Top: a GPS reading is required at the blue cross under the tree cover. However, a few metres to the east the sky is not obscured by trees: the accuracy of the fix here will be an order of magnitude better. Lower diagrams: the receiver has been taken into the open and a reading taken. A compass has then been used to site the actual location required and a measurement has been taken along the line between the two points; this can then be plotted back into the GIS later.



Plate 6 A query on GPS fixes from the Bogda Shan expedition: locations above 1,000 m are selected in a lighter colour (top half of the image); locations below 1,000 m are displayed but not selected (lower right of image).

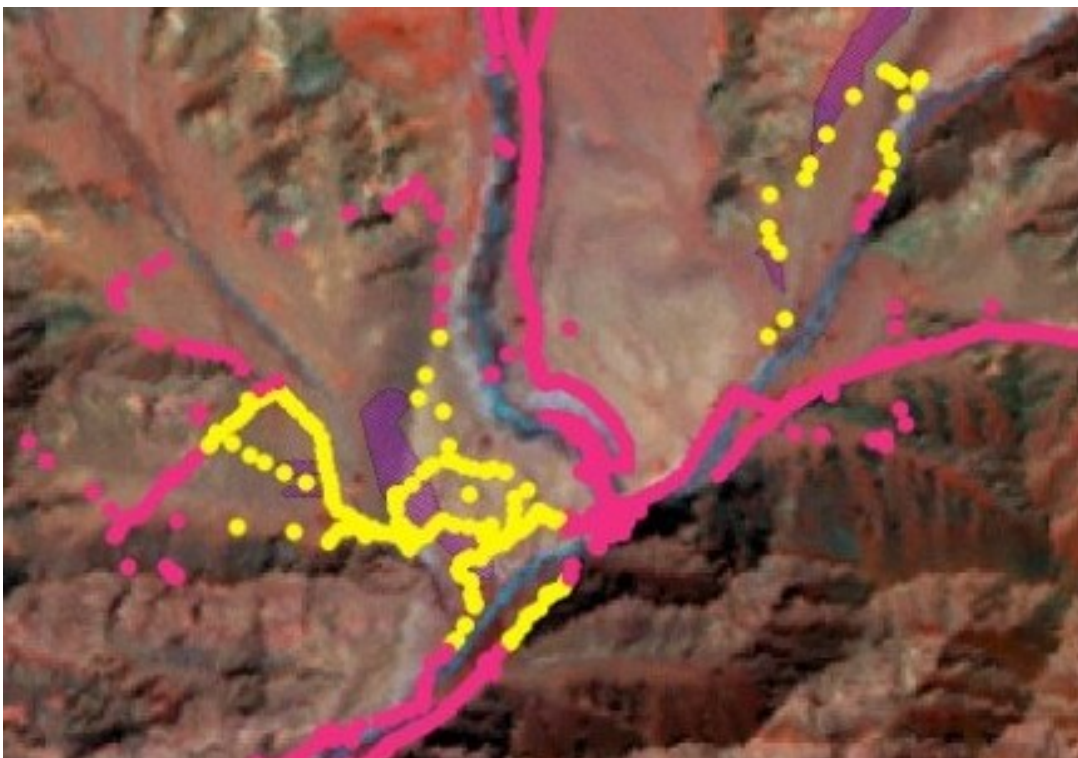


Plate 7 Results of a selection using a spatial query in the Bogda Shan GIS: GPS locations within 0.5 km of moraines are highlighted; moraine areas are shaded in grey.

Geological Map and Vector Overlay

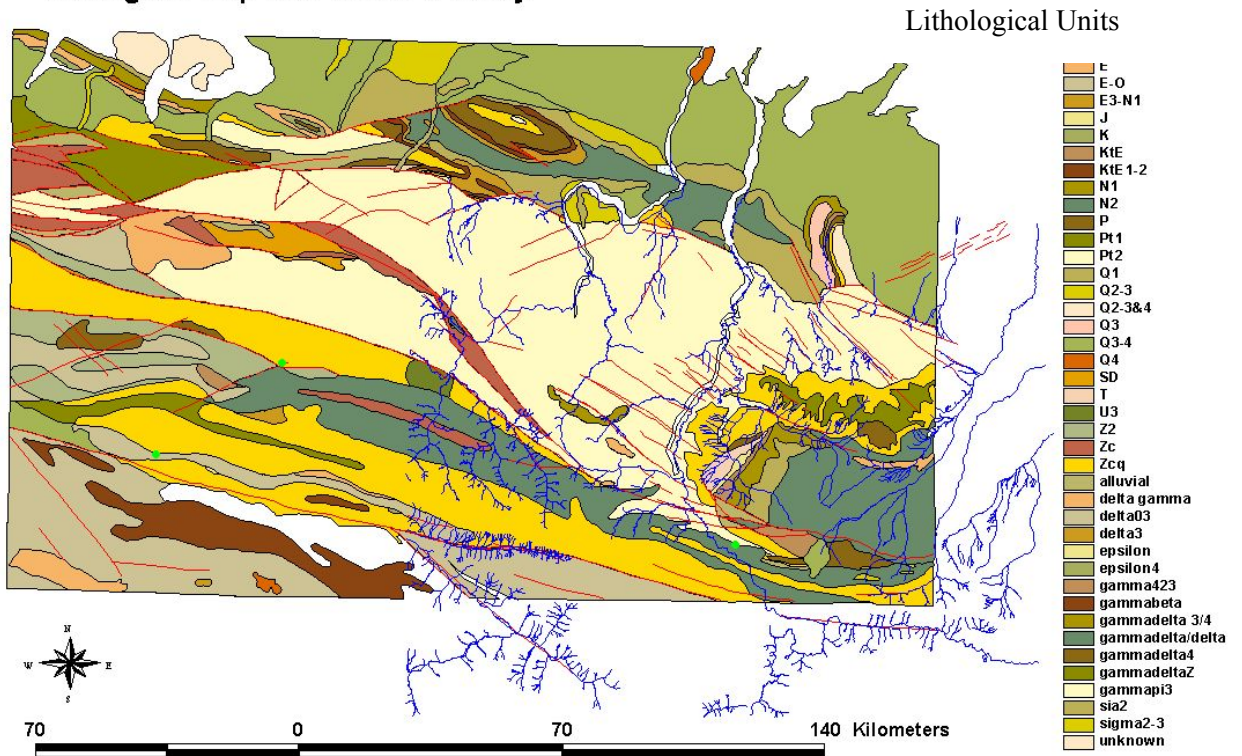


Plate 8 Vector layers showing rock units and drainage. Diagram from Whiteside, 2002.

Hotan Sub-Scene Showing Potential Jade Bearing Lithologies

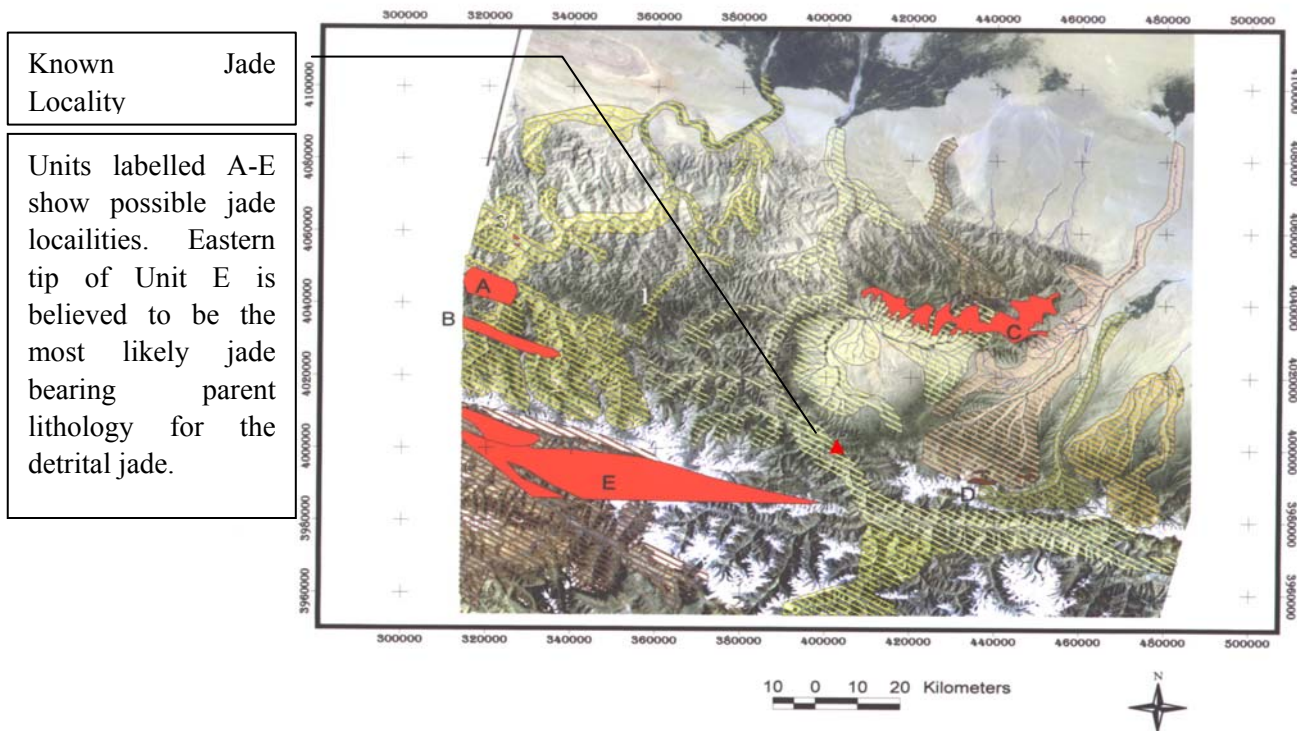
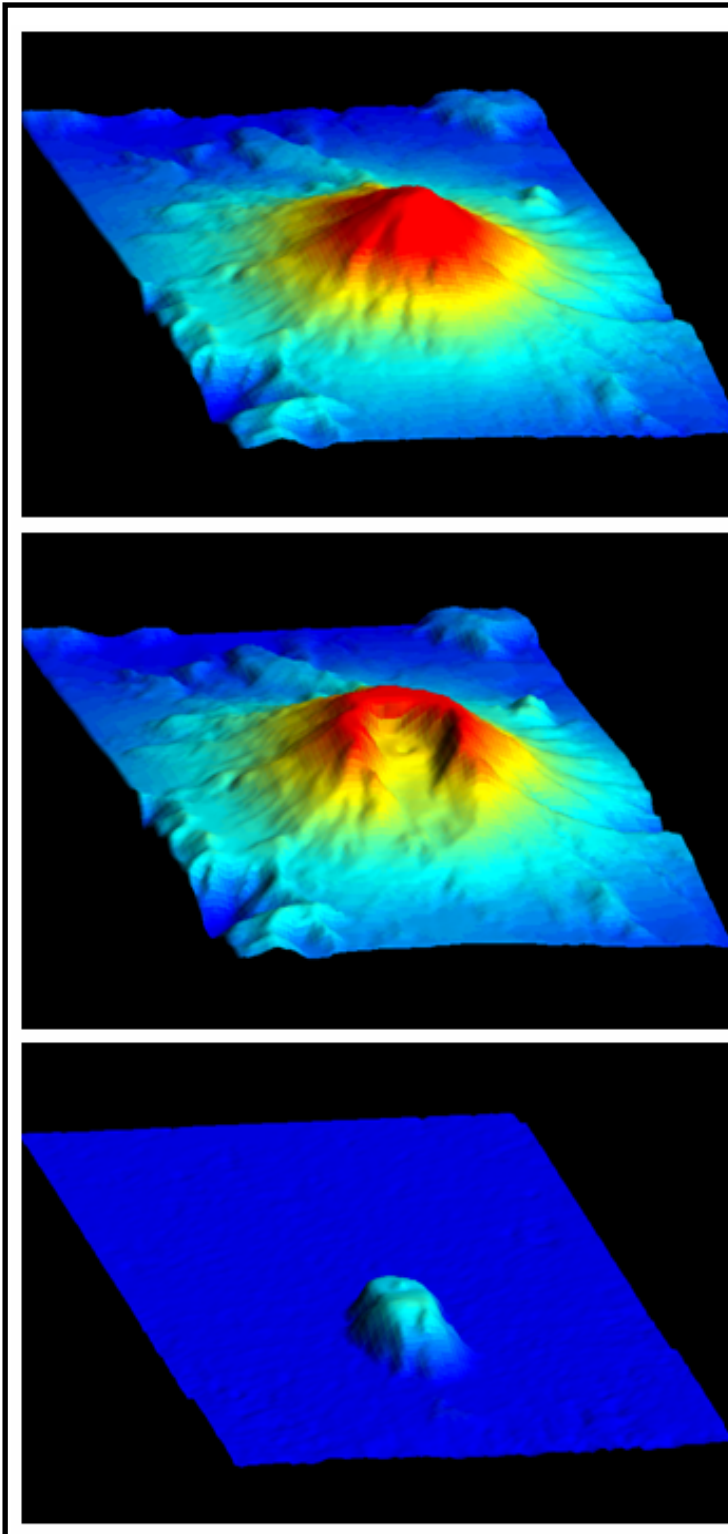


Plate 9 Finished GIS showing Likely Host Units (Moore et al. 2000).



In the first image we can see a 3D reconstruction of Mt St Helens before the May 1980 eruption. Note that in this image there has been no image overlay, that is all the colours and textures in the image are derived purely from height data. The colours represent height and north is to the bottom of the image.

In the second image we can see Mt St Helens after the blast. The northern flank of the volcano has collapsed removing large quantities of rock.

The amount of rock removed in the eruption can be very easily viewed in image processing software by using simple arithmetic processes (see Chapter 8) to subtract one volume from the other.

Plate 10 ER Mapper example data allows a 3D analysis of the Mt St Helens disaster of 1980.

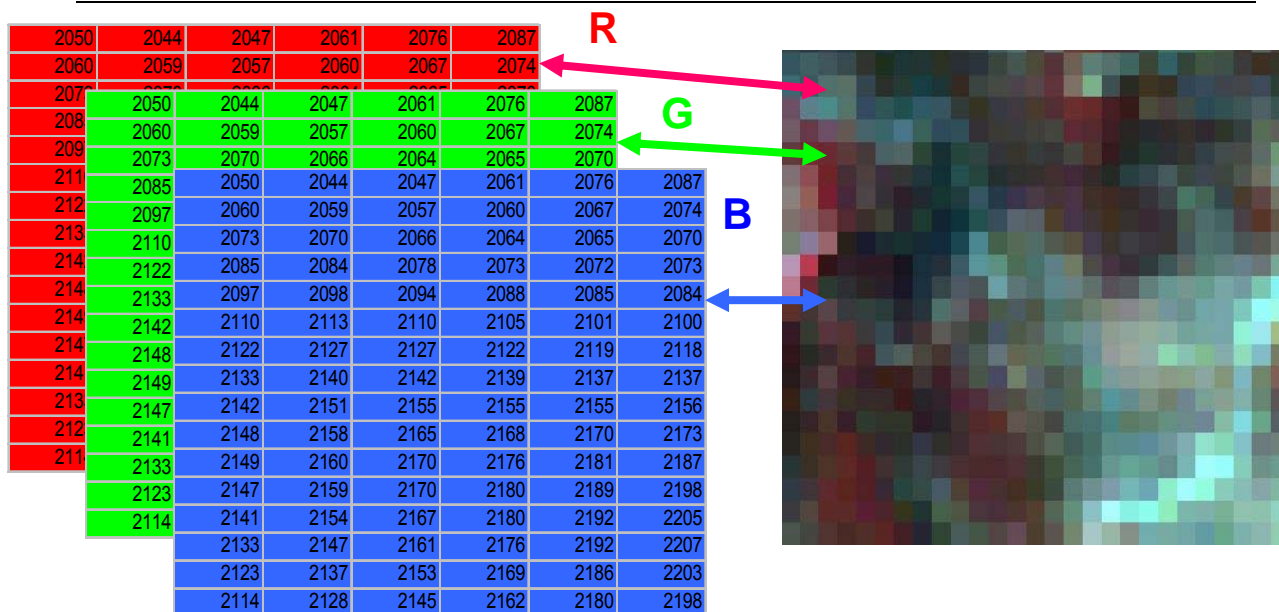


Plate 11 A colour digital image (right), produced by allocating three bands of an image to the red (R), green (G) and blue (B) colour-guns of a computer screen.

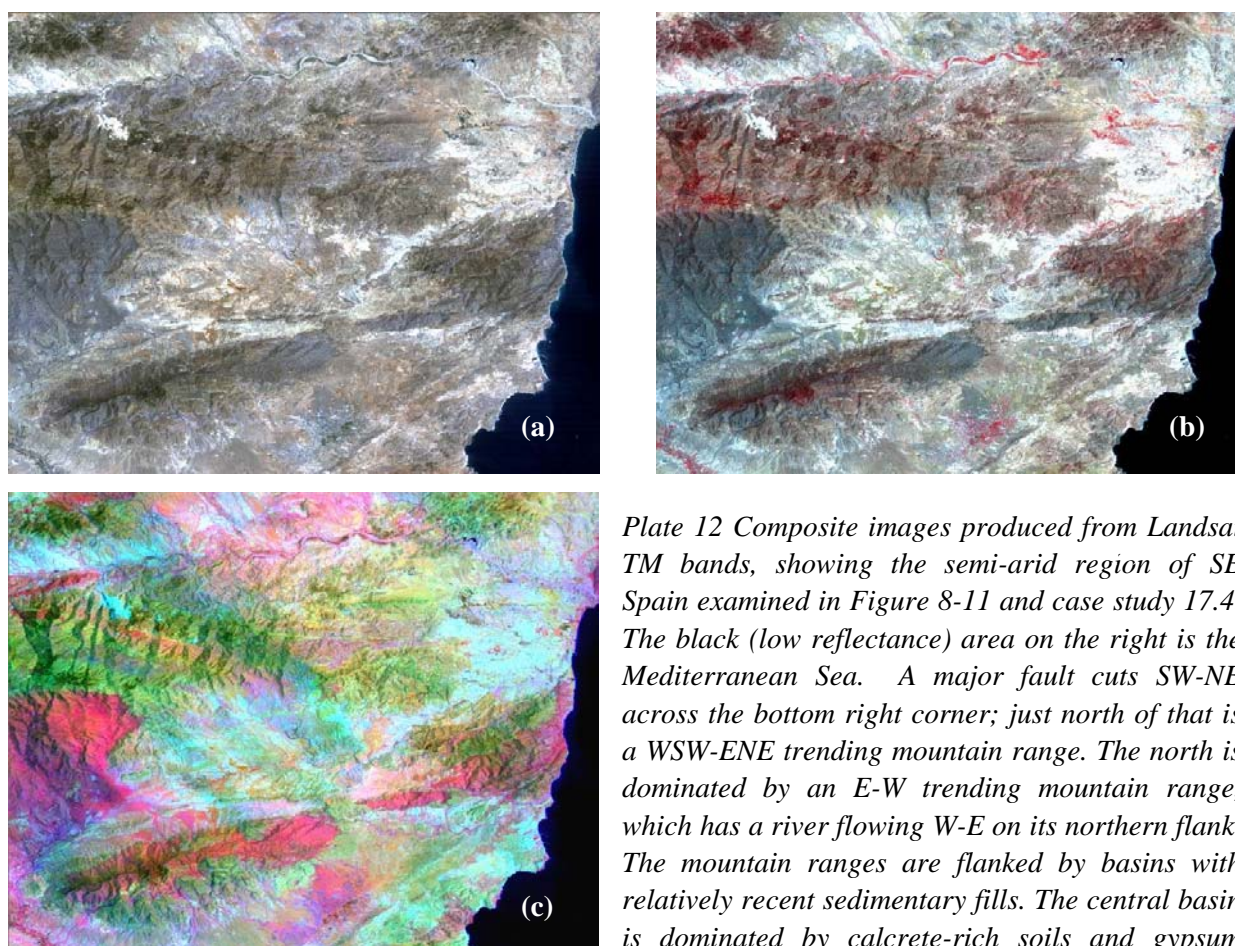
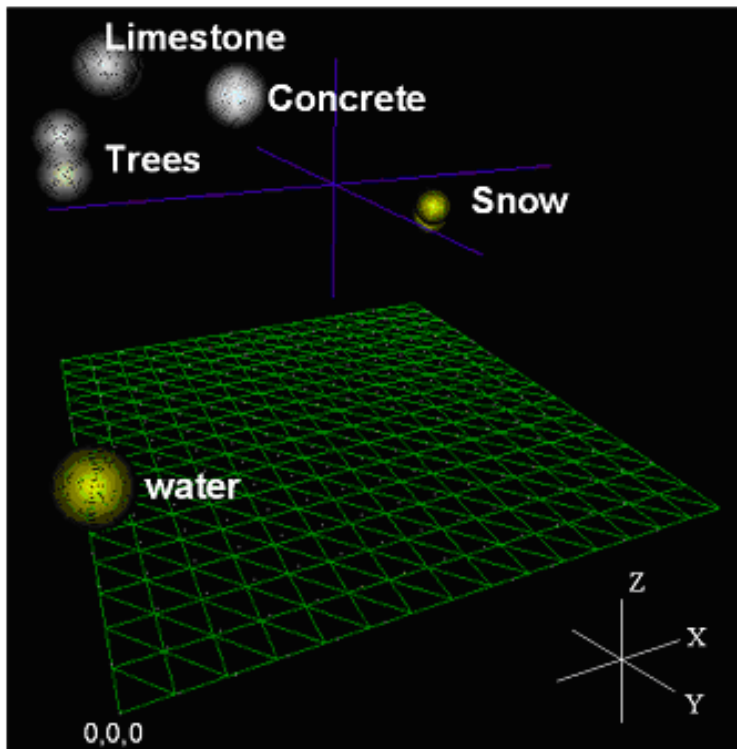


Plate 12 Composite images produced from Landsat TM bands, showing the semi-arid region of SE Spain examined in Figure 8-11 and case study 17.4. The black (low reflectance) area on the right is the Mediterranean Sea. A major fault cuts SW-NE across the bottom right corner; just north of that is a WSW-ENE trending mountain range. The north is dominated by an E-W trending mountain range, which has a river flowing W-E on its northern flank. The mountain ranges are flanked by basins with relatively recent sedimentary fills. The central basin is dominated by calcrete-rich soils and gypsum deposits, hence its dominant white colour (high reflectance); the western side of the central basin has been severely eroded, creating 'badland' terrain dominated by dark-coloured debris from adjacent hills. (a) 'True colour' (RGB321): the white areas are bare ground, mostly limestone, plus quarries of gypsum or marble; (b) 'False-colour infra-red': vegetation shows as red (irrigated agriculture or dense tree cover on the wetter mountains) or pink (sparse 'maquis' shrub cover); (c) RGB651: band 6, thermal infra-red, has been allocated the red colour gun – dark rocks and debris with a high thermal inertia show as shades of red, the hotter they are the stronger the red.



Landsat TM responses to various landcover types.

X Axis Band 1
Y Axis Band 4
Z Axis Band 5

Land Use	Band 1	Band 4	Band 5
Snow	98 %	87 %	3 %
Limestone	16 %	40 %	43 %
Trees	8 %	53 %	30 %
Water	3 %	3 %	2 %
Concrete	32 %	36 %	39 %

Table shows average reflectance (%) for land cover types in the listed bands of Landsat TM & ETM+

Plate 13 Schematic representation of trivariate classification, showing plots of reflectance values from Band 1 (blue), Band 4 (near infra-red) and Band 5 (mid infra-red) of Landsat Thematic Mapper. The various land cover types are now clearly distinguished.



Plate 14 A home experiment to recreate the perspective distortion of an air photo.

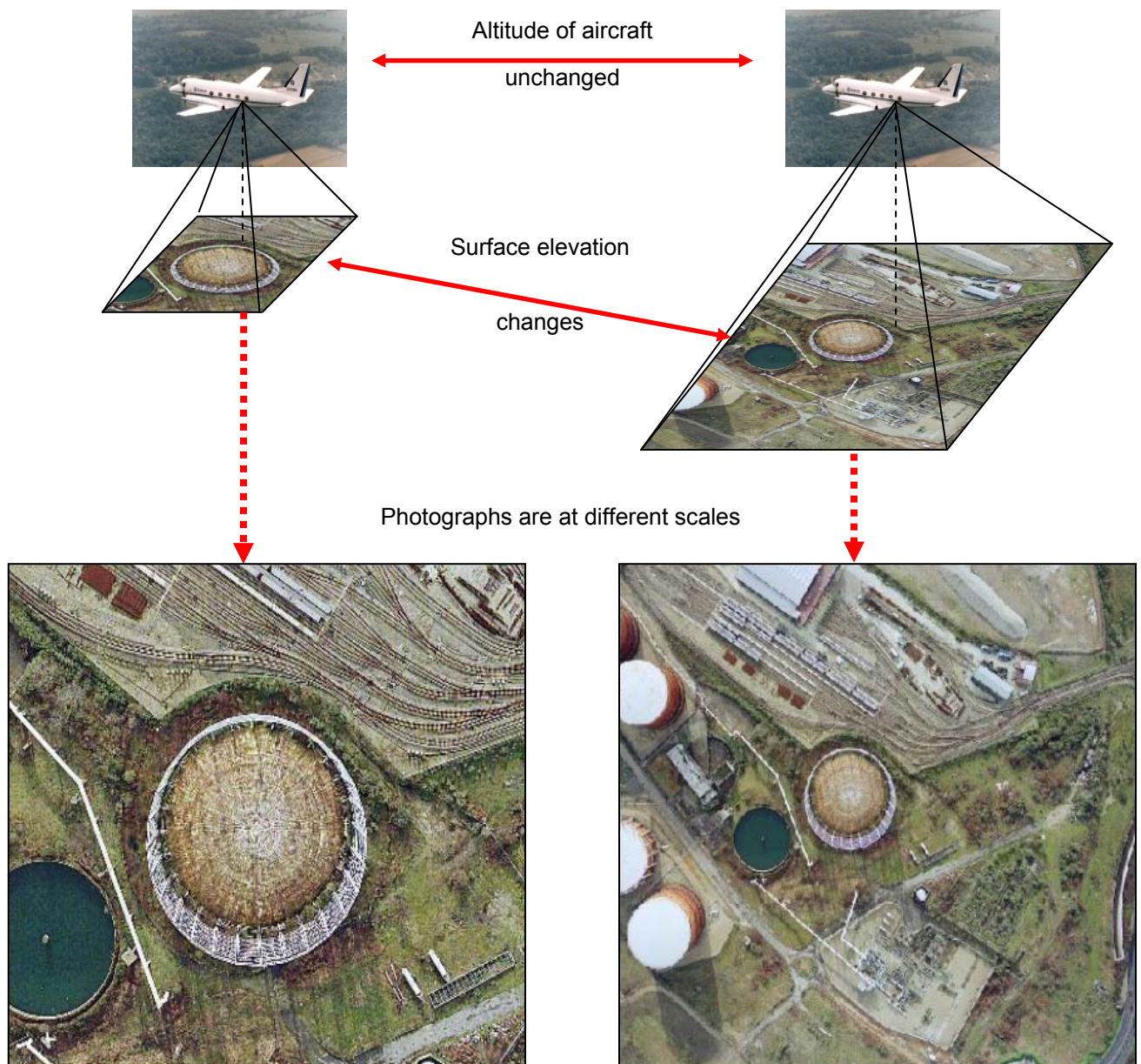


Plate 15 Illustration of the effect of terrain elevation on air photo scale.

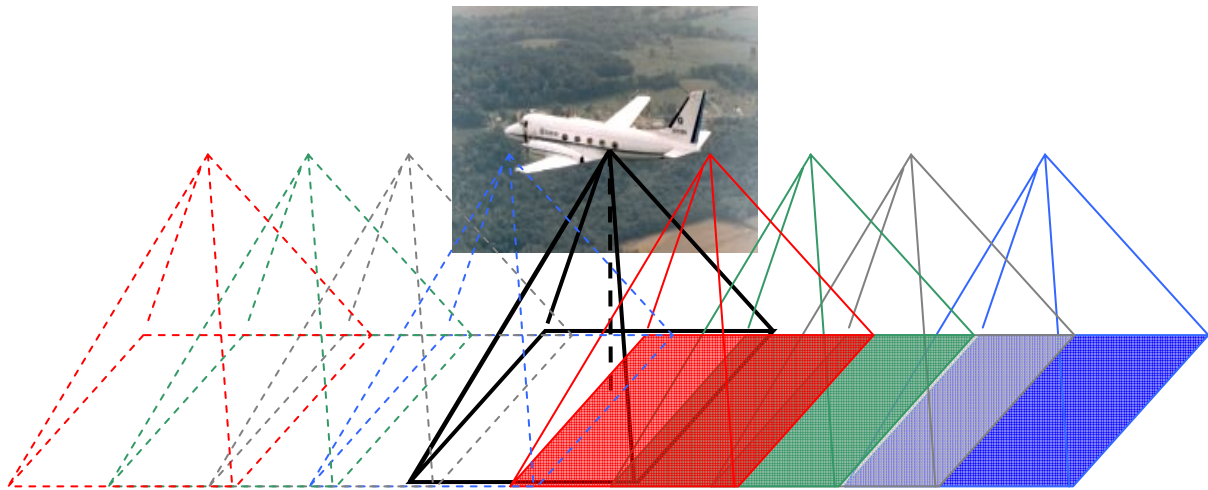
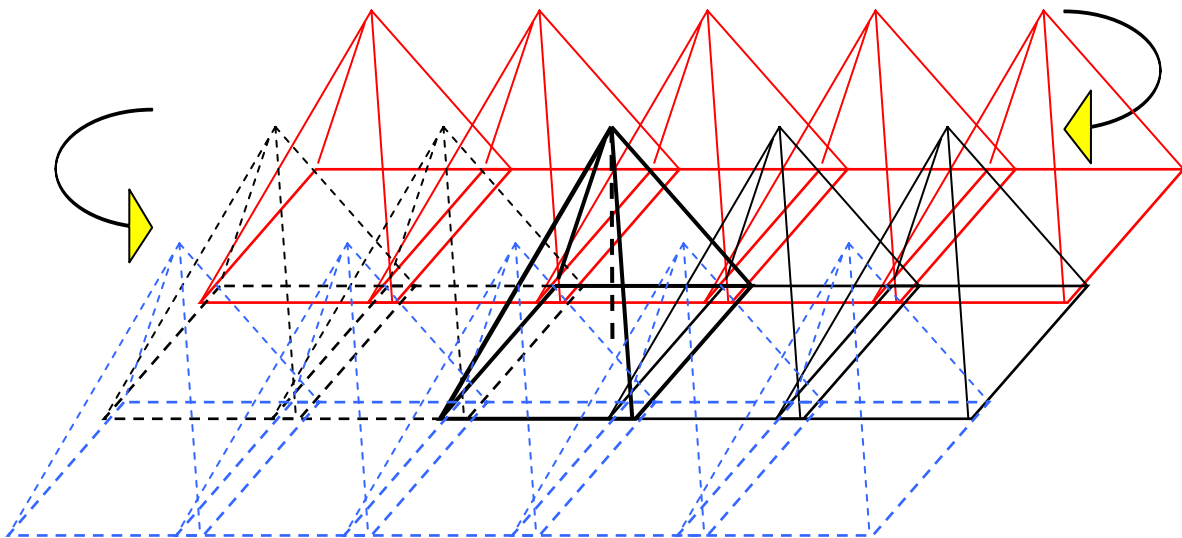


Plate 16

(Upper) Airphoto survey flight run showing coverage of each photo taken when acquiring coverage with 60% overlap between photos (solid lines show photos taken, dashed lines photos to be taken).



(Lower) Airphoto block of three runs showing coverage of each run and sidelap between runs. Solid black lines show photos taken, dashed lines show photos to be taken. Arrows show direction of flight (every other photo removed for clarity).

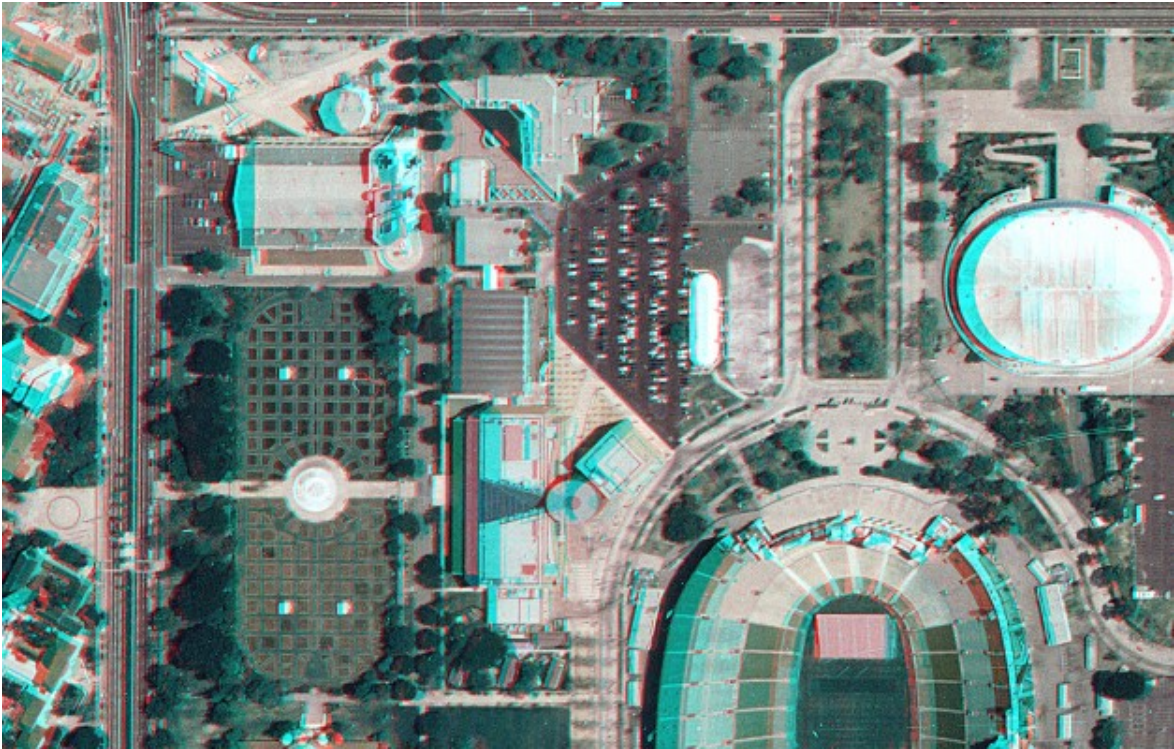


Plate 17 Anaglyph image showing two perspectives of an American football stadium and surrounding areas. Blue and red show the perspective differences between two co-located aerial photos. When viewed through blue/red glasses, the effect is a 3-D surface.

The screenshot shows a GIS application with several windows. The main window displays an aerial photo with numerous GCPs marked. The GCP tool window is open, showing a list of GCPs with their coordinates and residuals. The data table below is as follows:

Point #	Point ID	Color	X Input	Y Input						
17	GCP #17		76.362	-2471.						
18	GCP #18		136.650	-2627.						
19	GCP #19		255.870	-2634.						
20	GCP #20		499.573	-2597.151	529673.719	178174.694	Control	-1.100	0.743	1.327
21	GCP #21		723.506	-2497.201	529716.591	178224.395	Control	1.680	-3.150	3.570
22	GCP #22		1134.048	-2500.190	529813.577	178272.231	Control	-2.007	-0.167	2.014
23	GCP #24		1545.962	-2600.585	529923.017	178296.807	Control	-3.149	1.067	3.325
24	GCP #25		1403.343	-2563.852	529885.435	178289.017	Control	-0.522	0.600	0.795
25	GCP #26		1326.643	-2185.315	529823.386	178370.096	Control	-0.162	-1.647	1.695
26	GCP #27		1645.118	-2220.962	529903.179	178399.499	Control	-0.064	0.501	0.505

Plate 18 Creating Ground Control Points (GCPs) for an aerial photo from digital maps of central London. Note the columns for file co-ordinates and map co-ordinates.



Plate 19 Compass traverse and slope inclinometer survey in dense jungle, Guyana. Note the problem of inter-visibility: photo (b) is looking back along the survey line towards the surveyor in the white T-shirt (circled) of photo (a).



Plate 20 Integration of field notes, PC data and GPS points can be used to rectify imagery and create reliable and accurate expedition maps (photograph by Daniel Hourigan, 2001). Rectification points are best taken on easily identifiable points such as tight bends or junctions in roads.